Pergamon

Acta mater. Vol. 46, No. 1, pp. 327–340, 1998

PII: S1359-6454(97)00151-1
1359-6454/98 $19.00 + 0.00

SELF-ORGANIZATION IN THE INITIATION OF ADIABATIC SHEAR BANDS

V. F. NESTERENKO[1]†, M. A. MEYERS[1] and T. W. WRIGHT[2]

[1]Department of Applied Mechanics and Engineering Sciences, University of California, San Diego, La Jolla, CA 92037 and [2]U.S. Army Research Laboratory, Aberdeen Proving Ground, Maryland 21005, U.S.A.

(Received 30 June 1995; accepted 15 April 1997)

Abstract—The radial collapse of a thick-walled cylinder under high-strain-rate deformation ($\sim 10^4\ s^{-1}$) was used for the investigation of shear-band initiation and pattern development in titatium. Experiments were carried out in which the collapse was arrested in two stages, in order to observe the initiation and propagation of shear bands. The occurrence of shear bands to accommodate plastic deformation in response to external tractions is a collective phenomenon, because their development is interconnected. The bands were observed to form on spiral trajectories and were periodically spaced. The spacing of the shear bands decreased with the progression of collapse, and was equal to approximately 0.6 mm in the final stage of collapse. The shear-band spacing was calculated from two existing models, based on a perturbation analysis and on momentum diffusion. Values of 0.52 and 3.3 mm were obtained with material parameters from quasi-static and dynamic experiments. The predictions are found to give a reasonable first estimate for the actual spacings. The detailed characterization of the shear-band front leads to an assessment of the softening mechanisms inside a shear localization region. The initiation of localization takes place at favorably oriented grains and becomes gradually a continuous process, leading eventually to dynamic recrystallization. © *1997 Acta Metallurgica Inc.*

1. INTRODUCTION

Shear bands have been the object of research since the 19th century, when they were first observed and correctly interpreted by Tresca [1]. However, intense investigative efforts have only taken place since the second World War, and were triggered by the classic work of Zener and Hollomon [2]; studies [3, 4] have addressed both mechanistic and microstructural features of shear bands. It is recognized that shear localization is a very important and often dominating mechanism for plastic deformation in a number of materials especially at high strains and strain rates.

The behavior of shear bands is an essential part of the global high-strain-rate response of a material. Whereas the first mechanistic model of Recht [5] considered a simple balance between hardening and softening, more advanced treatments by Clifton [6], Bai [7], and Molinari and Clifton [8] introduced a perturbation analysis. Most studies were concerned with an isolated shear band, whereas the accommodation by internal plastic deformation in response to externally applied tractions takes place by the cooperative initiation and propagation of assemblages of shear bands. Some historical analogy with dislocations (the elementary carriers of plastic deformation at the microlevel) is suitable here. More recent efforts, dealing with self-organization and low-energy configurations of dislocations, are elucidating, in a quantitative manner, the plastic response of materials (e.g. Kuhlmann-Wilsdorf [9] and Kubin [10]).

A recurrent topic in studies of damage in materials is the question of spacing between damage sites. The ability to predict and possibly control significant features of the failure patterns, such as numbers, sizes, locations, and velocities of residual particles is dependent on a fundamental and quantitative understanding of evolution laws for these localized damage sites. A first step in obtaining an answer would be to estimate the spacing of initial nucleation sites since damage tends to grow in specific places in the material. Of course, this leaves out such questions as secondary damage and subsequent interaction of damage sites but it is still a crucial beginning.

The analyses carried out by Grady and Kipp [11], Wright and Ockendon [12], and Molinari [13] are theoretical efforts at elucidating the collective behavior of shear bands. The analysis by Grady and Kipp [11] is based on momentum diffusion as unloading occurs within the band and the one by Wright and Ockendon [12] and Molinari [13] uses perturbation of rate dependent homogeneous shearing; they are described in Section 3. Among other theoretical attempts to describe periodic propagating bands (shear band patterning) the approach by

†To whom all correspondence should be addressed.

Aifantis [14], based on the introduction of higher order gradients into the constitutive equation, should be mentioned. It is difficult to compare these predictions with experiments because of the lack of information on coefficients in the higher order terms, as well as the relatively arbitrary selection of a "dispersion" term, especially for essentially nonlinear problems.

The objectives of this paper are to report observations of shear-band assemblages obtained under controlled initiation conditions and to compare these observations with the Grady–Kipp [11] and Wright–Ockendon [12] models. The experimental data, in conjunction with parameters of the constitutive equation of the material under investigation, allow comparison with these or other theoretical approaches. The thick-walled cylinder technique, developed by Nesterenko and coworkers [15–18] was used, and the results are presented in Section 2.

2. EXPERIMENTAL PROCEDURE AND RESULTS

Figure 1(a) shows the experimental configuration used to produce the radial collapse of the metallic specimens. Commercial purity titanium (Grade 2, Altemp Alloys, CA) with equiaxed grains having an average size of 20 μm was used in the investigation. It was machined from 2 in. bar stock. The system was developed by Nesterenko and coworkers [15–18] and uses the controlled detonation of an explosive to generate the pressures required for the collapse of a thick-walled cylinder. The metallic specimens are placed within a copper driver tube; the system extremities are composed of steel plugs. The explosive is placed coaxially with the specimen and detonation is initiated at the top, propagating along the cylinder axis. An internal copper tube establishes the maximum collapse of the titanium tube. In the absence of copper, total collapse of titanium is obtained and the final radius is ~0.5 mm. Two different copper tube initial radii were used to arrest the collapse of the titanium at different stages.

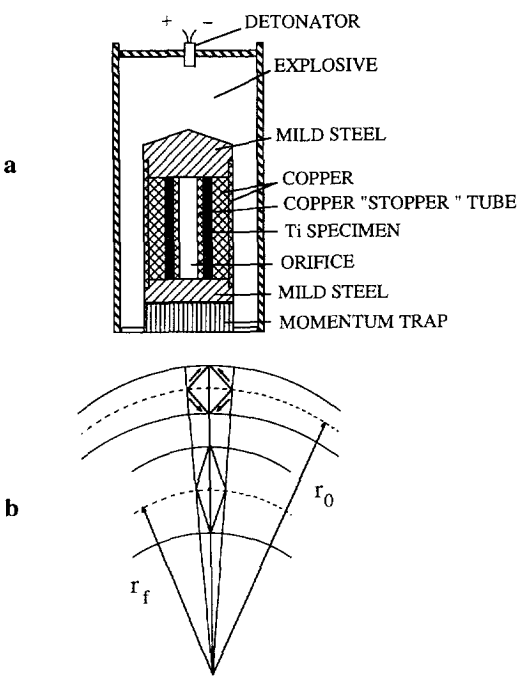

Fig. 1. (a) Experimental configuration for collapse of thick-walled cylinder and (b) pure shear deformation of an element as tube collapses.

The use of inner copper tube allows for "soft" termination of the collapse process and preserves the details of shear band geometry, especially the size of displacements on the inner radius of Ti. In these experiments, shear bands were not opened into cracks as was the case in previous experiments [19]. It also preserves the details of shear band structure and ensures that propagation of shear bands is not replaced by propagation of cracks developing from shear bands during elastic unloading. To arrest the collapse at different radii, central rods with different radii were also used. However, the impact of Ti inner surface, having a structure developed by shear bands, with the rods destroys details of the shear bands.

The explosive parameters in the thick-walled cylinder method (detonation velocity, density, and thickness) were carefully selected to provide "smooth" pore collapse; wave reflection effects are minimized and spalling of the internal cylinder surface is nonexistent. An explosive with low detonation velocity ($D \approx 4000$ m/s) with initial density 1 g/cm^3 was used in the experiments. A description of the method can be found in [15–19]. The velocity of the inner wall of the tube was measured by an electromagnetic gage, described by Nesterenko and Bondar [16, 17].

The state of stress generated within the collapsing cylinder before shear localization starts is one of pure shear. This is shown in Fig. 1(b), in which the distortion of an elemental cube of radius r_0 is followed as it moves towards the axis of the cylinder. The strain in the axial direction is zero, and there is no rotation of the elemental cube. The planes of maximum shear lie at 45° to a radius, as indicated at r_0 in Fig. 1(b), and remain unrotated as deformation proceeds inwards, at least until shear bands develop.

As the tube is collapsed inwards, its inner surface experiences increasing strains which tend to infinity as radius of the cavity $R_f \to 0$. These experiments were carried out by Nesterenko *et al.* [19] and reveal the shape, spacing, and configuration of shear bands after complete collapse of the cylinder. Thus, this technique is well suited for the study of both shear-band initiation and propagation. For the specimen dimensions used in the current investigation the initial radii of the internal copper cavity,

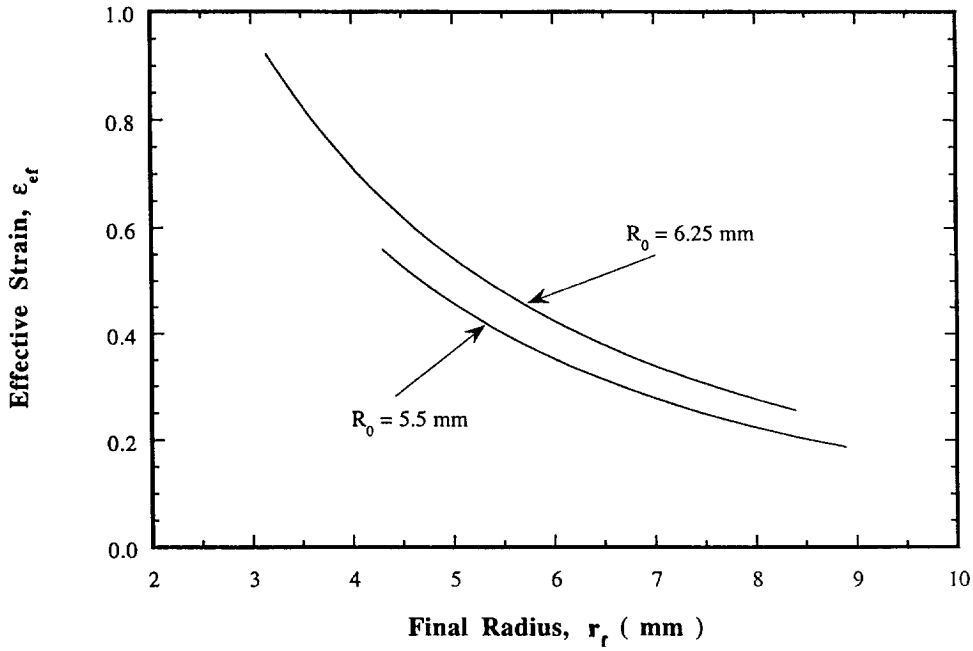

Fig. 2. Effective strain in Ti as a function of radius in partially collapsed geometry for two configurations: $R_0 = 5.5$ mm (smaller collapse strain) and $R_0 = 6.25$ mm (larger collapse strain).

R_0, were equal to 5.5 and 6.25 mm with internal radius of Ti cylinder equal to 7 mm for both cases. This provided two values for the maximum shear strain in the Ti specimens.

The radial, tangential, and axial strains for this geometry are given by:

$$\varepsilon_{rr} = \ln\left(\frac{r_0}{r_f}\right) \quad \varepsilon_{\phi\phi} = -\ln\left(\frac{r_0}{r_f}\right) = -\varepsilon_{rr} \quad \varepsilon_{zz} = 0. \quad (1)$$

The radii r_0 and r_f (Fig. 1(b)), representing the initial and final positions of a general point, are related by the conservation of mass, if deformation is uniform:

$$r_0^2 - R_0^2 = r_f^2 - R_f^2. \quad (2)$$

The effective strains

$$\varepsilon_{ef} = \frac{2}{\sqrt{3}}\varepsilon_{rr} = \frac{2}{\sqrt{3}}\ln\frac{r_0}{r_f}$$

for material points being collapsed to different final radii r_f are depicted on Fig. 2 for the initial radii $R_0 = 5.5$ mm and $R_0 = 6.25$ mm. Each line designates the strain of a material point as it converges inward. The extremity of the line designates the radius and strain of the inside surface, after the collapse was arrested.

The strain rate for a general material point can be evaluated from the radial velocity of the cylindrical cavity $v(t)$, which was measured by an electromagnetic technique [16. 17]. The insertion of Ti cylinders inside a copper driver tube, shown in Fig. 1(a), does not significantly change the time of collapse in comparison with the uniform copper cylinder having the same geometrical dimensions, because the replacement of the central part of the copper by Ti cylinders changes the overall mass (and initial velocity) by no more than 20%. That is why the velocity data obtained for a monolithic copper cylinder can be used, as a first approximation, to calculate the strain rate. For example, for a point on the inner cavity, the following relationship is used to calculate the shear strain rate at 45° to the radius:

$$\dot{\gamma} \approx 2\dot{\varepsilon}_{rr} = 2\frac{1}{R}\frac{dR}{dt} = 2\frac{v(t)}{(R_0 - \int_0^t v(t)dt)}. \quad (3)$$

Fig. 3 shows the shear strain rates during the collapse process for two points corresponding to two

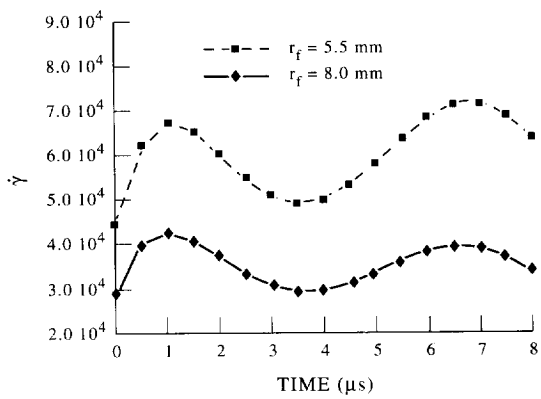

Fig. 3. Shear strain rate vs time for different final radii ($r_f = 5.5$ mm; $r_f = 8$ mm).

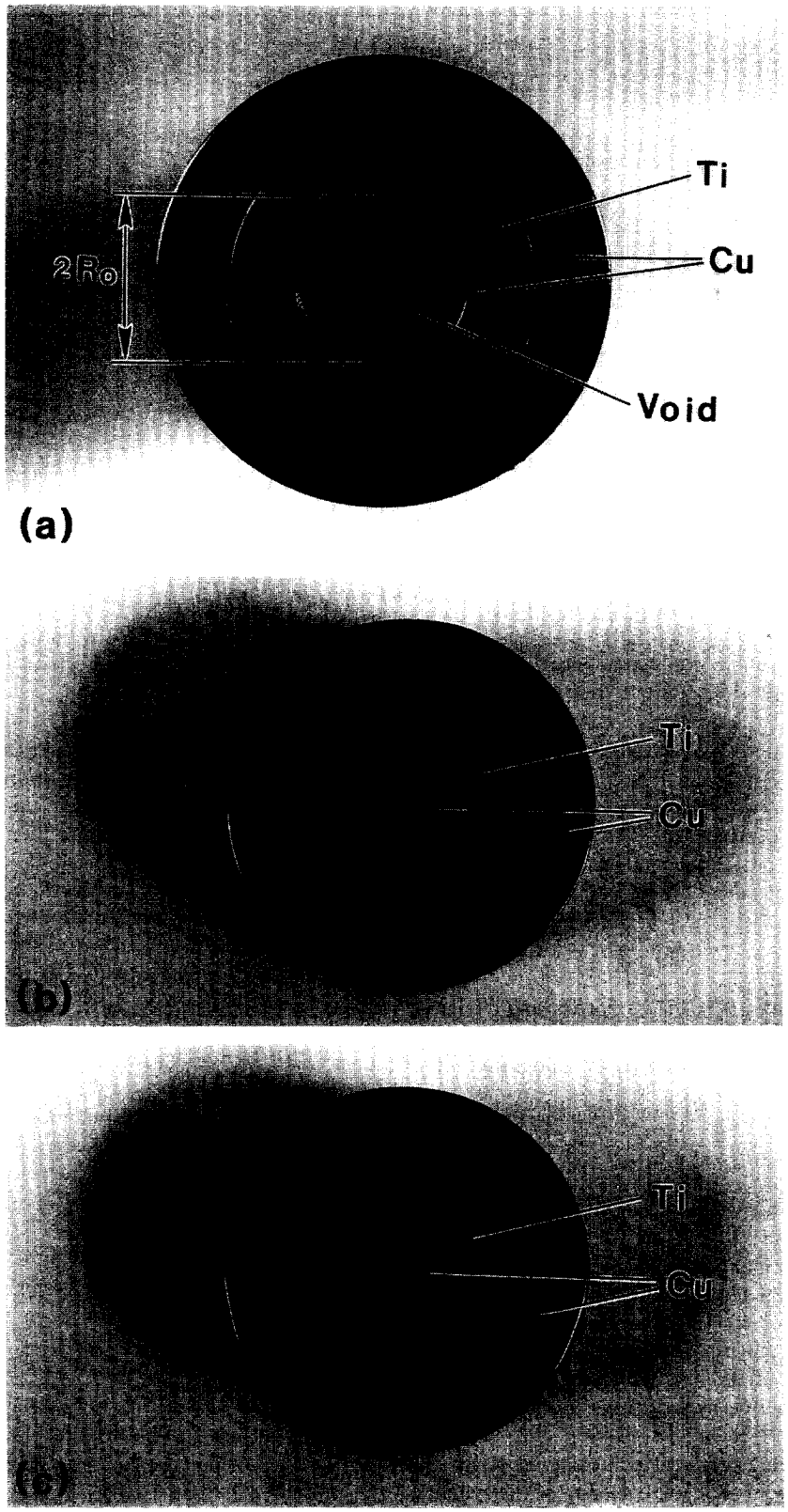

Fig. 4. (a) Initial and (b, c) collapsed configurations of titanium specimens; (b) $R_0 = 5.5$ mm; (c) $R_0 = 6.25$ mm.

value of final radii, which are the ends of shear bands in Ti. The strain rate is seen to fluctuate around corresponding mean value and the variation (±15%) is not significant. That is why, to a first approximation, the strain rates for these material points can be considered as constant and equal to $3.5 \times 10^4\ s^{-1}$ and $6 \times 10^4\ s^{-1}$.

Figure 4 shows the (a) initial, and (b) and (c) final configurations of specimen cross-sections. The copper "stopper" tubes, which have initial internal radii R_0 equal to 5.5 and 6.25 mm, are completely collapsed by the implosion, subjecting the titanium tube to two levels of plastic strain.

Three different experiments were carried out for each condition. They are labeled M1, M2, and M3 for the first set and M4, M5, and M6 for the second set. The reproducibility of the shear-band patterns observed is clearly shown in Figs 5 and 6. The radii $R_0 = 5.5$ and 6.25 mm were chosen based on observed strains for shear-band propagation by previous studies. Meyers *et al.* [20] obtained shear-band propagation in commercial purity titanium (grain size 72 μm; Grade 2), for an effective strain between 0.2 and 0.45. This was determined in a Hopkinson bar using hat-shaped specimens. Previous experiments by Nesterenko *et al.* [19] on the same Ti revealed that the effective strain for shear-band propagation was equal to 0.22. For the two experimental setups used in the current research, the effective strains can be readily calculated.

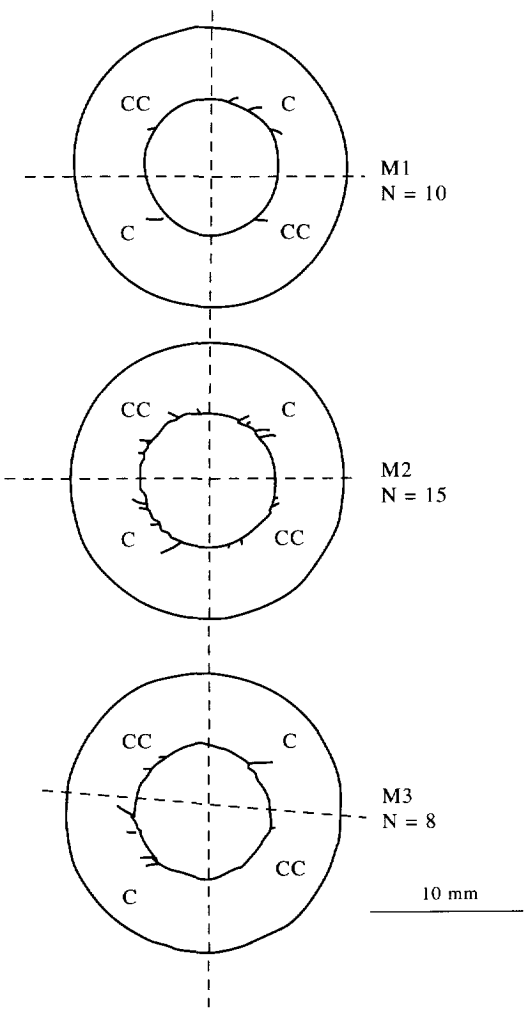

Fig. 5. Shear-band traces for three different experiments $R_0 = 5.5$ mm; C and CC represent regions of clockwise and counterclockwise dominances, respectively.

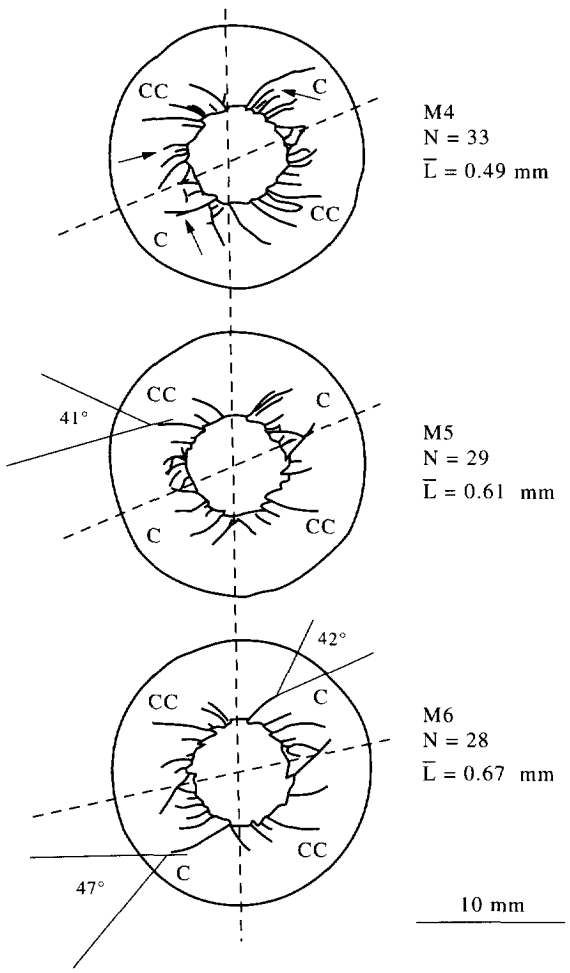

Fig. 6. Shear-band traces for three different experiments $R_0 = 6.25$ mm; C and CC represent regions of clockwise and counterclockwise dominances, respectively.

$$\varepsilon_{ef} = \frac{2}{\sqrt{3}}\,\varepsilon_{rr} = \frac{2}{\sqrt{3}}\ln\frac{r_0}{r_f}. \tag{4}$$

Since $r_0^2 - R_0^2 = r_f^2$ and $r_0 = 7$ mm, then the strains for the collapsed inner surface of Ti with two initial sizes of inner copper tubes are:

For $R_0 = 5.5$ mm $\quad \varepsilon_{ef} = 0.554$ at $r_f = 4.5$ mm.

For $R_0 = 6.25$ mm $\quad \varepsilon_{ef} = 0.923$ at $r_f = 3.3$ mm. (5)

The value of $\varepsilon_{ef} = 0.554$ should provide strains higher than those required for initiation according

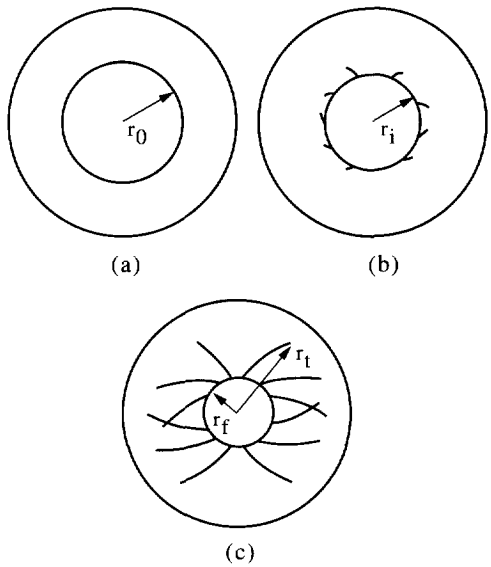

Fig. 7. Schematic sequence of events during collapse of cylinder; (a) initial configuration, (b) initiation of shear-band formation and (c) spiral propagation of shear bands during collapse.

to [19, 20], whereas $\varepsilon_{ef} = 0.923$ should provide a well-developed shear-band pattern. This is exactly borne out by the observations shown in Figs 5 and 6. The following observations can be made:

(a) The shear bands initiate at the internal surface of the titanium specimen and propagate outwards;

(b) The angle of the extremities of the shear bands with the radial directions fluctuates around 45°, which is the plane of maximum shear stress (and strain). This is shown for three shear bands in Fig. 6.

(c) Both clockwise and counterclockwise spirals are observed, in contrast with earlier observations by Nesterenko *et al.* [19]. Figure 6 shows that these clockwise and counterclockwise spirals organize themselves into four families. They are marked C and CC in Fig. 6. The differences between the present results and those of Nesterenko *et al.* [19] are not completely understood and could be due to pre-existing texture in the titanium specimens under current investigation, which is revealed by anisotropy of plastic deformation in compression tests.

(d) The number of shear bands increases with plastic strain. The number of shear bands (N) counted at the internal surface of the cylinder is marked in Figs 5 and 6. It was possible to estimate an average spacing between the shear bands for experiments M4, M5, and M6, where the pattern was well established. This spacing was calculated considering only shear bands with the same orientation, either clockwise (C) or counterclockwise (CC). The average spacings between the shear bands, also marked in Fig. 6, are $L = 0.49$, 0.61, and 0.67 mm for specimens M4, M5, and M6, respectively. The averaging procedure was made for a number of shear bands equal to 25, 23 and 23. This procedure can cause some decrease in real shear-band spacings (up to 27%) as a result of their actually unknown nucleation radius, which in any case should be between radii of inner Ti tube equal to 4.5 mm (Fig. 5) and 3.3 mm (Fig. 6).

(e) Some shear-band bifurcation is observed in Fig. 6; it is marked by arrows.

The initiation and propagation of shear bands during the collapse is schematically shown in Fig. 7. When the internal radius of Ti sample (initial value equal to r_0, Fig. 7(a)), reaches a value r_i, the critical shear strain for shear band initiation is attained (Fig. 7(b)). Upon further collapse, the shear bands grow outward (Fig. 7(c)).

The experiments cannot track exactly the shear strain at which shear bands initiate. Nevertheless, the small size of the shear bands in Fig. 5 shows clearly that the effective strain of 0.554 is slightly above the minimum strain for the initiation.

The global strains at the tips of the bands (at r_t, Fig. 7c) were also calculated. Figure 8 shows the distribution of strains at the shear-band tips. For the initial collapse ($R_0 = 5.5$ mm, Fig. 8(a)), the minimum strain at the shear-band extremity is equal to 0.35 and they range from 0.35–0.5. For the well-developed shear bands (Fig. 8(b),

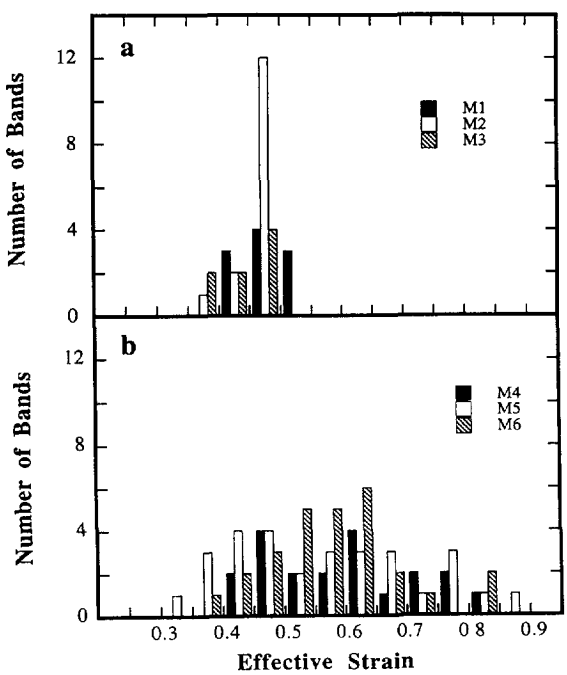

Fig. 8. Distribution of global effective strains at tips ($r = r_t$) of bands for two different radii; (a) $R_0 = 5.5$ mm; (b) $R_0 = 6.25$ mm.

$R_0 = 6.25$ mm), the minimum strain is actually the same (0.3), but a wider distribution of strains 0.3–0.9 is observed. The minimum strain at the tip of the shear band is consistent with the calculated initiation strain, which was estimated to range from 0.2–0.45 [20]. It is also consistent with earlier results by Nesterenko *et al.* [19]: $\varepsilon_{ef} = 0.22$.

The radial span of the shear bands was measured and correlated with the height of the steps at the internal surface, Δ. The results are shown in Fig. 9. More developed shear bands create a larger step.

The results shown in Figs 5–9 enable the conclusion to be made that shear bands start to form at an effective strain equal to 0.3 along the internal surface of the hollow cylinder. As the collapse proceeds, the number of shear bands increases. The distribution in the radial spans of the shear bands is a direct consequence of their gradual formation: the bands that form first propagate farther outward.

3. ANALYTICAL PREDICTIONS OF SHEAR BAND SPACING

In the present experimental configuration the simplest question to be posed is the number of initial sites for shear localization to be expected around the circumference of the inner surface as the cylinder collapses.

A preliminary answer may be given by simply adopting the result for spacing given by Grady and Kipp (GK) [11] for rate independent materials or the more recent analysis developed by Wright and Ockendon (WO) [12] for rate dependent materials. Both results were derived for one-dimensional shearing of an infinite strip of material without regard to boundary conditions. Therefore, the application to the present case is only approximate.

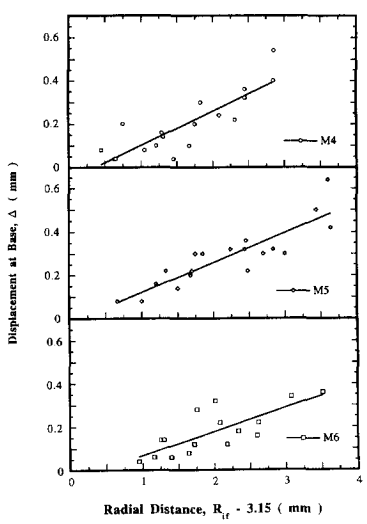

Fig. 9. Relationship between displacement at internal cylinder surface, Δ, and radial range of shear bands, for experiments with $R_0 = 6.25$ mm.

Nevertheless, it is important from dimensional considerations alone to find the appropriate nondimensional groupings of physical quantities. The two approaches will be reviewed and compared.

The basic notion, used in the GK analysis, is that rapid loss of strength or ability to transfer shearing stresses across the developing shear band affects neighboring material by forcing it to unload. This unloading process is communicated outward by momentum diffusion, rather than by elastic wave propagation, and ultimately the minimum separation between independently nucleating bands arises from computing the distance traveled by the unloading front during the time required to unload as localization occurs. Their analysis also assumes that the width of the shear band adjusts itself so as to achieve a maximum growth rate, the growth rate of narrower bands being limited by thermal diffusion and that of wider bands by inertia. The details of the analysis are too complex to repeat here, but the predicted spacing, L_{GK}, given in their Equation (23), with suitable changes in notation (thermal diffusivity χ has been replaced by thermal conductivity divided by density and heat capacity, $k/\rho C$), is:

$$L_{GK} = 2(9kC/\dot{\gamma}^3 a^2 \tau_0)^{1/4} \tag{6}$$

In this formula the applied shear strain rate is $\dot{\gamma}$, and the relation between flow stress and temperature is assumed to be

$$\tau = \tau_0[1 - a(T - T_0)] \tag{7}$$

where τ_0 is the strength at a reference temperature T_0, and a is a softening term. GK did not include strain and strain-rate hardening in their analysis.

On the other hand, the WO analysis [12] is based on the notion that shear bands arise from small, but growing disturbances in an otherwise uniform region of constant strain rate. Disturbances do not propagate in perpendicular directions, but simply grow in place, so the most likely minimum spacing is obtained by finding the fastest growing wavelength. The problem is posed by first finding the uniform fields and then by finding differential equations for perturbations with the uniform fields taken as the ground state. Fourier decomposition of the perturbation equations is followed by an asymptotic representation of the solution. Then it is a simple matter of differentiation to find the wavelength that grows the fastest.

WO assumed the following constitutive equation, which has both thermal softening and strain-rate hardening components:

$$\tau = \tau_0[1 - a(T - T_0)]\left(\frac{\dot{\gamma}}{\dot{\gamma}_0}\right)^m. \tag{8}$$

$\dot{\gamma}_0$ is a reference strain rate and m is the strain-rate sensitivity. τ_0 is the flow stress at the reference temperature T_0 and strain rate $\dot{\gamma}_0$.

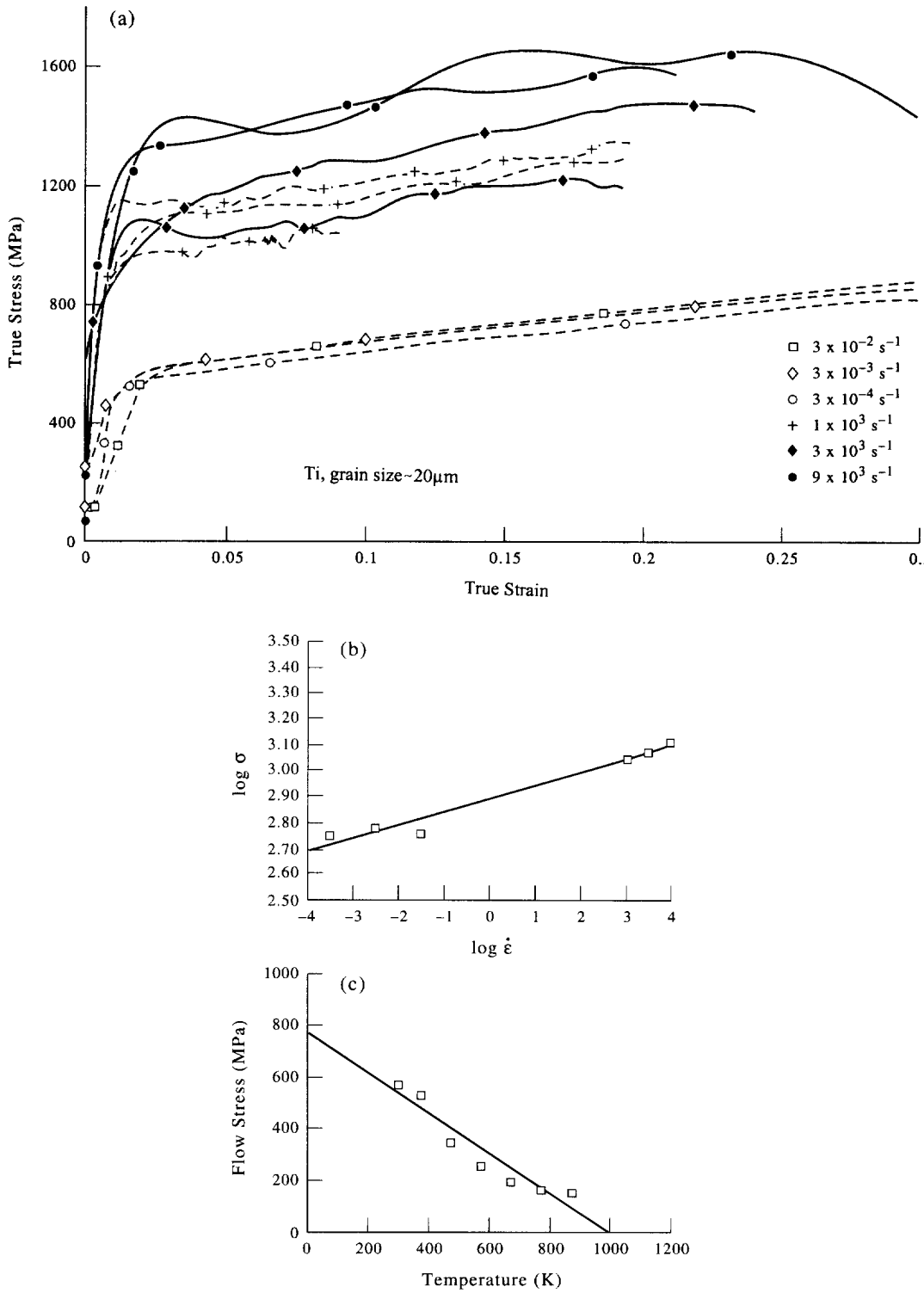

Fig. 10. Experimentally obtained stress–strain response for titanium; (a) stress–strain curves, (b) strain-rate sensitivity and (c) thermal softening (from Meyers *et al.* [20]).

WO arrived at an expression for the wavelength providing maximum growth of the perturbation. This provides a shear-band spacing, L_{WO}, equal to:

$$L_{WO} = 2\pi\left(\frac{kCm^3\dot{\gamma}_0^m}{\dot{\gamma}^{3+m}a^2\tau_0}\right)^{1/4}. \quad (9)$$

Although the approaches taken by GK and WO are completely different, the former concentrating on the stress collapse mechanism due to well developed shear bands, and the latter concentrating on the earliest stages of localization where shear bands are practically absent being represented by nucleation sites, it is a remarkable fact that, except for numerical factors and the rate constants, the two results are similar. The assumed flow laws in equations (7) and (8) differ only by the rate factor, and as a consequence the major difference between equations (6) and (9) is that strain rate sensitivity appears strongly in the numerator and weakly in the denominator of equation (9) (for most metals, $m \ll 1$), whereas it does not appear at all in equation (6), and that the dependence on strain rate is slightly weaker in equation (6) than in equation (9). On the other hand, there are only a finite number of ways that the constants may be combined to obtain a length scale (but there are certainly more than one) e.g. $(\tau_0 C^2\dot{\gamma}^{m-3}/\dot{\gamma}_0^m ka)^{1/2}$, $(k/\rho C\dot{\gamma})^{1/2}$, $(\tau_0\dot{\gamma}^{m-2}/\dot{\gamma}_0^m\rho)^{1/2}$, as well as that found in equation (9), so it is not quite so surprising as it initially seemed that the results are so similar.

The GK and WO formulations were applied to the materials tested in Section 2 by means of the use of equations (6) and (9), respectively. They enabled the calculation of the shear-band spacings L_{GK} and L_{WO}, respectively.

Mechanical tests were performed on titanium specimens at low and high strain rates in order to obtain the parameters of the constitutive equations used by GK and WO. The mechanical response at ambient temperature is shown in Fig. 10(a). The strain rate sensitivity m can be obtained from data presented in Fig. 10(b) and is equal to 0.052. The thermal softening parameter a was obtained from data by Meyers *et al.* [20] on a similar alloy (Grade B, titanium with grain size of 72 μm). The linear fit to the thermal softening data is shown in Fig. 10(c); $a = 10^{-3}$ K^{-1} in the temperature range of 300–1,000 K.

The physical parameters in the GK and WO models and the calculated shear-band spacings L_{GK} and L_{WO} are presented in Table 1 ($\tau_0 = \sigma_0/2$ where σ_0 is the yield stress in uniaxial loading). It is seen that both models provide estimates of L which are in agreement with the experimental results within one order of magnitude; the WO and GK predictions are 0.52 and 3.3 mm, respectively. The WO analysis predicts spacings L that are approximately one sixth of the GK calculations. The experimentally obtained spacings (L = 0.6 mm after averaging over the entire experimental results) are in excellent agreement with predictions of the WO model. Considering the one-dimensional character of the models and three-dimensional geometry of experiments, the neglecting of work hardening, the agreement of theoretical predictions of WO model with experimental results should be considered cautiously. The recent calculations by Molinari [13] incorporate work hardening and predict a shear-band spacing for Ti equal to 0.75 mm, also in good agreement with experimental results reported here.

It should be mentioned that the WO model describes only the minimum spacing between initiation sites for shear bands, whereas the GK model describes the spacing of fully formed bands. If the spacing of shear bands is determined by their initiation, the WO model should be obeyed. On the other hand, if the propagation stage establishes the spacing, the GK model should dominate. It seems clear that the WO analysis successfully predicts the initiation for Ti. On the other hand, the bifurcation of the shear bands observed in Fig. 6(c), is possibly indicative of a momentum–diffusion (GK) process: once the bands reach a spacing above a critical value, new bands are formed to accomplish deformation.

4. EXTREMITIES OF SHEAR BANDS

The two models predicting shear band spacings are qualitatively different and reflect the different stages of shear band development. In this context, it is instructive to look at the tip of the shear bands to identify the possible mechanism of their formation and subsequent self-organization into patterns.

Detailed observation of the tips of the shear bands enables the identification of the progressive mechanisms of plastic deformation as the strain increases. The well-formed shear bands are clearly visible by scanning electron microscopy as regions with a thickness of 10–20 μm with sharp boundaries and with a microstructure that is only resolvable by transmission electron microscopy. Indeed, Grebe *et al.* [21], Meyers and Pak [22], and Meyers *et al.* [23] were able to clearly identify microstructure consisting of recrystallized grains of 0.1–0.3 μm diameter,

Table 1. Material parameters and theoretical predictions of shear–band spacing, L, for Ti

Material	m	τ_0 (MPa)	k(J/s m K)	C(J/kg K)	a(K^{-1})	$\dot{\gamma}_0$ (s^{-1})	L_{OW} (mm)	L_{GK} (mm)
Ti	0.052	280	19	528	10^{-3}	10^{-3}	0.52	3.3

with a fairly low dislocation density. A specific mechanism for recrystallization was proposed and discussed extensively [23, 24]. The extremities show a gradual progression of plastic deformation leading to well-developed bands. Figure 11 shows a montage of the shear-band tip with larger magnifications of the fully formed band (left-hand side), as well as the onset regions. These regions show an alternation of sharp localization (center top) with more gradual deformation (center bottom). These alternations occur on the grain-size scale and indicate that the tip of the band is evidently affected by the local crystallography of plastic deformation. The crystallographic aspects are lost in fully formed bands. Some grains localize preferentially at the tip of the band. Subsequently, less localized regions connect more localized grains. As these regions join up, they form a band. These irregularities at the front contribute to the deviations of the shear-band trajectories. Figure 12 shows, in a schematic fashion, the configuration of the shear-band tips as they are envisaged at this point. For clarity, the shear-band tip is divided into three regions: I—intermittent, II—deformed; III—recrystallized. The approximate lengths of the two precursor regions (100 and 400 μm) are also shown in this plot. The initiation of shear-band formation takes place in favorably oriented grains, and is initially discontinuous. These shear-band segments gradually join up and form a continuous front.

Zhou *et al.* [25, 26] investigated the initiation and propagation of shear bands in a Ti–6 Al–4 V alloy. They were able to measure the temperature within the band and found that it rose to values of 750 K at an impact velocity of 64.5 m/s. They were also able to establish the velocity of propagation of the shear-band tips. For an impact velocity of 64.5 m/s, the propagation velocity was equal to approximately 50–75 m/s. In the experiments carried out in this research program it is also possible to estimate a minimum velocity of propagation of the shear bands. The collapse process of the internal void takes place in the time interval of approximately $t = 8$ μs [17]. The most extensive shear bands show a radial extension of approximately $r_t = 6.8$ mm at $r_f = 3.3$ mm. This is shown in Figs 7 and 9. These values enable the estimation of a growth velocity:

$$v = \frac{-r_f + \sqrt{2r_t^2 - r_f^2}}{t\sqrt{2}}. \tag{10}$$

The shear band is approximated by a straight line growing at a 45° angle to the radial direction. A velocity of 500 m/s is obtained. The actual velocity is higher, since the initiation of the shear bands requires a critical plastic strain. This value of the propagation velocity is higher by an order of magnitude than the velocity measured by Zhou *et al.* [25, 26]. Hence, the propagation velocity should not be considered a fixed value, but depends on the external loading.

It is important to connect the WO and GK models to microstructural processes happening in the material. Possible micromechanisms for the initiation of shear bands have been discussed by Meyers *et al.* [20]. Local fluctuations in strain and temperature lead to the initiation. Additionally, the surface of the inner cylinder wall contains imperfections which lead to perturbations. A few possible microstructural initiation sites are shown in Fig. 13; they are all at grain scale. They are briefly discussed below. There is always a distribution of grain sizes within a material, and larger grains exhibit a lower yield stress (σ_1, in Fig. 13), whereas smaller grains have a higher yield stress (σ_2 in Fig. 13). The large grain will deform preferentially and could be an initiation site. Grain rotation can lead to softening, which is shown schematically in Fig. 13(b). The increase in Schmid factor of a grain with plastic deformation leads to localized softening which can initiate a shear band. The localized deformation of one grain can propagate along a band as shown in Fig. 13(c). This mechanism of localization through the cooperative plastic deformation of grains has been modeled by Peirce, *et al.* [27] and Anand and Kalidindi [28]. A fourth mechanism is shown in Fig. 13(d). A dislocation pile-up, upon bursting through a grain boundary, can generate the local temperature rise and plastic deformation which would initiate shear band. This mechanism has been proposed by Armstrong and Zerilli [29].

The temperature rise accompanying shear localization can lead, eventually, to microstructural rearrangements of a significant nature. Stage III in Fig. 12 shows the formation of a different microstructure. It is instructive to calculate the temperature rise within a shear band as a function of plastic shear. The Johnson–Cook constitutive equation provides a ready means of doing this. Figure 14 shows the adiabatic stress–strain curves at three different strain rates: 10^3, 10^4, and 10^5 s^{-1}. The temperature rise as a function of plastic strain are also shown. A broad range of strain rates was used to incorporate the changes of strain rate occurring when the shear band forms: the local strain rate is much higher than the global strain rate. The temperature inside the shear band rises to 700–800 K when the shear strain is one. Strains larger than one can produce dynamic recrystallization in titanium, which requires 0.4 T_m, where T_m is the melting point (= 1943 K). Indeed, dynamic recrystallization has been previously identified [20, 23–25] within shear bands.

We can conclude that crystallographic peculiarities play a very important role in shear band initiation and are absent in both models (GK and WO). Nesterenko, Bondar and Ershov [17] observed that a decrease of initial grain size in copper from 1000 μm to 100 μm did not alter the num-

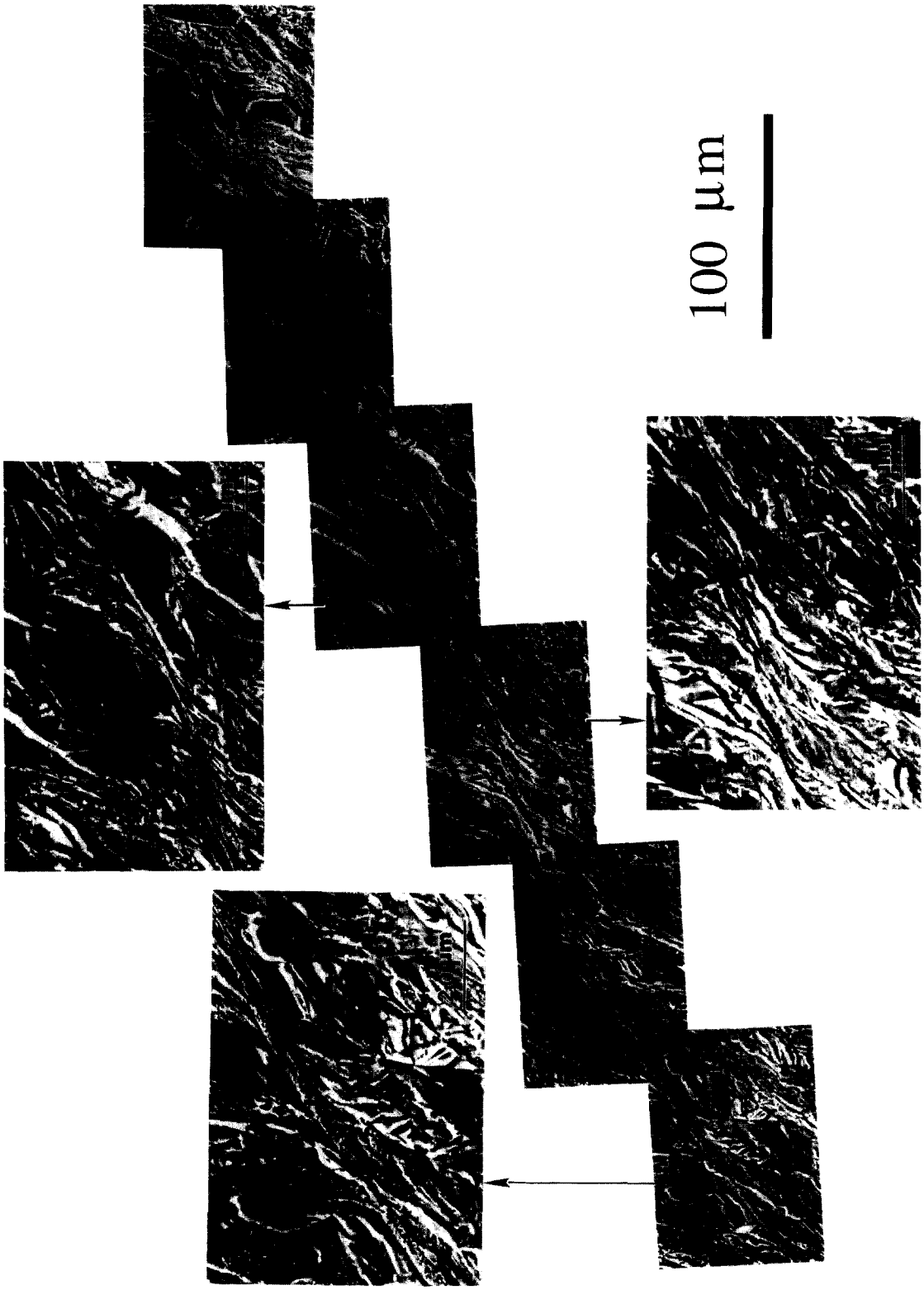

Fig. 11. Montage of SEM micrographs of a shear-band tip showing different regions.

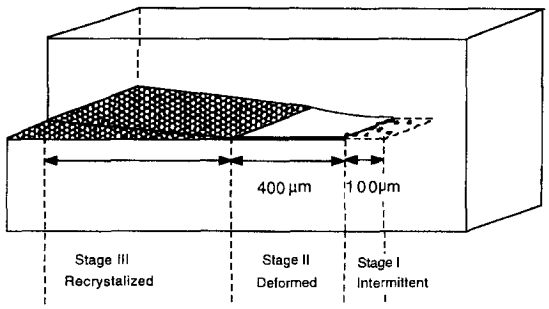

Fig. 12. Schematic representation of regions at the tip of a shear band.

ber of shear bands; however a further decrease from 100 μm to 30 μm resulted in an increase in the number of shear bands from 30 to 50 under the same conditions of loading as the current work, with an attendant decrease of shear band spacings. This tendency cannot be explained with the help of the GK model because the reduction in grain size cannot provide the eight-fold increase of the initial yield strength required to explain the decrease of spacings by a factor of 1.7 (equation (6)). A possible explanation of this result in the WO model can be connected with a difference in strain-rate sensitivity of yield strength in materials with different grain sizes.

The synergism between the continuum softening and the existence of microstructural initiation sites might have a bearing on the shear-band spacing and should be explored. A possible explanation for the success of the continuum modeling for shear band spacings is that self-organization of shear bands is developed at a stage where thermal softening and heat conductivity play dominant roles in stress collapse.

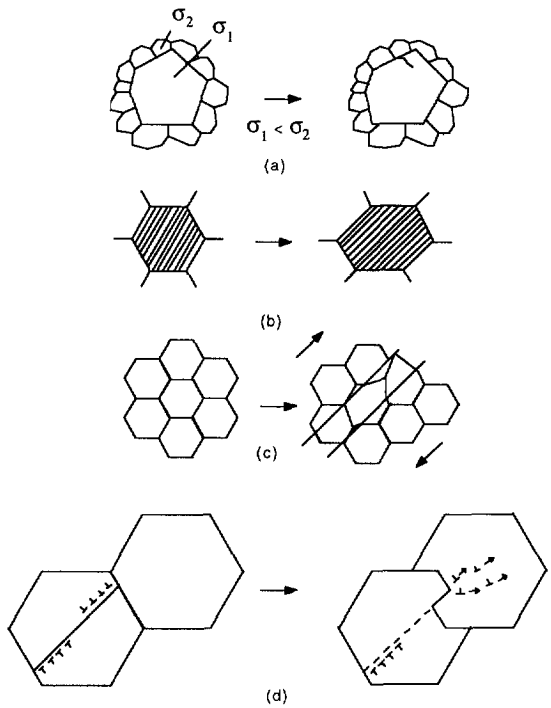

Fig. 13. Possible shear-band initiation mechanisms in single-phase homogeneous materials. (a) grain-size inhomogeneity, (b) geometrical softening, (c) Peirce–Asaro–Needleman textural localization and (d) dislocation pile-up release.

5. SUMMARY AND CONCLUSIONS

It has been experimentally demonstrated, using the high-strain radial collapse of thick-walled cylinders of titanium, that shear bands undergo a self-organization process as they initiate and propagate. The partial collapse of a thick-walled cylinder generates controlled and reproducible plastic deformation gradients under a state of stress of pure shear. The self-organization of shear bands manifests itself in the formation of an array of shear bands that diverge from the initiation region on the internal surface of the thick-walled cylinder, that is periodic, and that has a characteristic spacing.

The experimental results are compared with predictions of two models:

(a) The Grady–Kipp model [11] is based on momentum diffusion: the formation of a shear band produces an unloading of the adjacent regions that is a function of the rate of softening. These unloaded areas are shielded from subsequent initiation/propagation of shear bands.

(b) The Wright and Ockendon model [12] is based on a perturbation analysis in one-dimensional shear. In this analysis, the spacing of shear bands is governed primarily by the strain-rate sensitivity and thermal softening of the material.

The experimentally obtained shear band spacing in Ti (0.6 mm) is in good agreement with the predictions of the Wright and Ockendon model (0.52 mm). It is felt that the OW theory better predicts the shear band patterning if it is mainly determined by the initiation stage, whereas the propagation is affected by the momentum diffusion in the GK approach. Prior to the onset of localization, momentum diffusion is absent, and its role is only fully felt in the propagation stage.

Possible microstructural relations to shear-band initiation and propagation sites are analyzed. The connection between shear-band spacing at initiation and grain size, which provides favorably oriented sites, is discussed.

The self-organization and collective behavior of shear bands is essential in the accommodation of

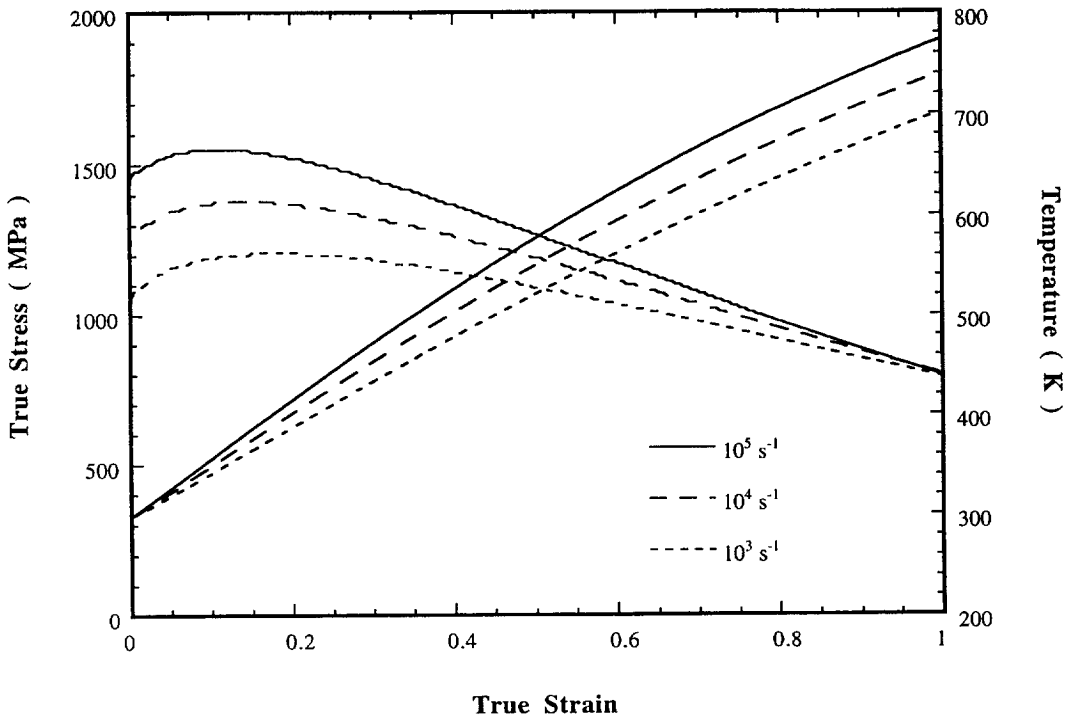

Fig. 14. Thermal excursion within shear band, assuming adiabaticity (values computed using Johnson–Cook constitutive equation); calculation for 10^3, 10^4, 10^5 s^{-1} shown.

large plastic strains at high strain rates, and the methodology developed herein can be extended to a wide variety of materials. The present results also clearly demonstrate that material instability is very important in cylindrical pore collapse and is the main reason for breaking symmetry of this process.

Acknowledgements—This research is supported by the U.S. Army Research Office, Contract DAAH 04-94-G-031, by the U.S. Office of Naval Research, Contract N00014-94-1-1040 (Program Officer J. Goldwasser) and by the U.S. Army Research Laboratory. Authors wish to acknowledge the valuable help in conducting experiments by S. Usherenko, Minsk.

Note added in proof—The existence of an intermittent zone at the tip of a brittle fracture was proposed by W. Gerberich (ASTM STP 945, 1988, p. 5) who called it the semi-cohesive zone. Individual grains in this zone could cleave if favorably oriented. The concepts of the intermittent zone (proposed here) and the semi-cohesive zone (proposed by Gerberich) are similar.

REFERENCES

1. Tresca, M. H., *Proc. Inst. Mech. Engrs.*, 1878, **30**, 301.
2. Zener, C. and Hollomon, J. H., *J. Appl. Phys.*, 1944, **15**, 22.
3. Bai, Y. Dodd B. 1992. Adiabatic Shear Localization. Pergamon, Oxford, UK. 302, 303, 305, 332, 333, 352.
4. 1994. Mechanics of Materials. (Special issue on Shear Instabilities and Viscoplasticity Theories) 17.
5. Recht, F. R., *J. Appl. Mech.*, 1974, **31**, 189.
6. Clifton, R. J., in *Material Response to Ultra High Loading Rates* Rep. NMAB-356, NMAB, NAS, Washington, DC, Chapter 8, 1979.
7. Bai, Y., in *Shock Waves and High-Strain-Rate Phenomena in Metals: Concepts and Applications*, ed. by M. A. Meyers and L. E. Murr, p. 227, Plenum, NY 1981.
8. Molinari, A. and Clifton, R. J., *C. R. Acad. Sci. Paris*, 1983, **296**, 1.
9. Kuhlmann-Wilsdorf, D., *Met. Trans.*, 1985, **11A**, 2091.
10. Kubin, L. P., *Phys. Stat. Sol.*, 1993, **135**, 433.
11. Grady, D. E. and Kipp, M. E., *J. Mech. Phys. Solids*, 1987, **35**, 95.
12. Wright, T. W. and Ockendon, H., *Int. J. Plasticity*, 1996, **12**, 927.
13. Molinari, A., Collective Behavior and Spacing of Adiabatic Shear Bands. *J. Mech. Phys. Sol.* (to be published).
14. Aifantis, E. C., *Int. J. Engng Sci.*, 1992, **30**(10), 1279.
15. Nesterenko, V. F. and Bondar, M. P., *DYMAT Journal*, 1994, **1**, 245.
16. Nesterenko, V. F. and Bondar, M. P., *Combustion, Explosion, and Shock Waves*, 1994, **30**, 500.
17. Nesterenko, V. F., Bondar, M. P. and Ershov, I. V. 1994. Instability of Plastic Flow at Dynamic Pore Collapse. High-Pressure Science and Technology-1993, ed. S. C. Schmidt, J. W. Shaner, G. A. Samara and M. Ross. AIP Conference Proceedings. pt. 2. p. 1173.
18. Nesterenko, V. F., Meyers, M. A., Chen, H. C. and LaSalvia, J. C., *Applied Physics Letters*, 1994, **65**, 3069.
19. Nesterenko, V. F., Meyers, M. A. and Wright, T. W., in *Metallurgical and Materials Applications of Shock Wave and High-Strain-Rate Phenomena*, ed.

bib_vol_nr;L. E. Murr, K. P. Staudhammer and M. A. Meyers, 397, Elsevier Science, Oxford, 1995.
20. Meyers, M. A., Subhash, G., Kad, B. K. and Prasad, L., *Mechanics of Materials*, 1994, **17**, 175.
21. Grebe, H. A., Pak, H-r and Meyers, M. A., *Metall. Trans.*, 1985, **16A**, 761.
22. Meyers, M. A. and Pak, H-r, *Acta Met.*, 1986, **34**, 2493.
23. Meyers, M. A., LaSalvia, J. C., Nesterenko, V. F., Chen, Y. J. and Kad, B. K., in *Third Int. Conf. on Recrystallization and Related Phenomena*, ed. T. R. McNalley. Monterey, 1997, p. 279.
24. Nesterenko, V. F., Meyers, M. A., LaSalvia, J. C., Bondar, M. P., Chen, Y. J. and Lukyanov, Y. L., *Matls. Sci. and Eng.*, 1997, **A229**, 23.
25. Zhou, M., Rosakis, A. J. and Ravichandran, G., *J. Mech. Phys. Sol.*, 1996, **44**, 981.
26. Zhou, M., Ravichandran, G. and Rosakis, A. J., *J. Mech. Phys. Sol.*, 1996, **44**, 1007.
27. Peirce, D., Asaro, R. J. and Needleman, A., *Acta Met.*, 1984, **31**, 1951.
28. Anand, L. and Kalidindi, S. R., *Mech. of Mat.*, 1994, **17**, 223.
29. Armstrong, R. W. and Zerilli, F. J., *Mech. of Mat.*, 1994, **17**, 319.